**Online at:** https://researchtrendsjournal.com
**Indexed Journal**

**ISSN No:** 2584-282X
**Peer Reviewed Journal**


**INTERNATIONAL JOURNAL OF TRENDS IN EMERGING RESEARCH AND DEVELOPMENT**

**Volume 3; Issue 5; 2025; Page No. 01-16**

**Received: 02-06-2025**
**Accepted: 10-07-2025**
**Published: 03-09-2025**

# Bond characteristics of recycled scrap metal based milled reinforcing steel bars with reference to deformations of self-compacted concrete beams in sustainable construction

**[1]John Kwesi Quarm Junior, [2]Charles K Kankam, [3]Edward C Mansal, [4]Russel O Afrifa and [5]Jack O Banahene**

[1]Directorate of Physical Development and Estate Management, University of Cape Coast, Ghana
[2-5]Department of Civil Engineering, College of Engineering, Kwame Nkrumah University of Science and Technology, Kumasi, Ghana

**DOI:** https://doi.org/10.5281/zenodo.17047420

**Corresponding Author:** John Kwesi Quarm Junior

**Abstract**

The interaction between reinforcing steel and its surrounding concrete plays a decisive role in the strength, safety, and service life of reinforced concrete structures. In this study, the bond–slip behavior of steel bars manufactured in Ghana was examined when embedded in self-compacting concrete (SCC) and normal concrete (NC). Controlled pull-out tests were carried out using 12 mm, 16 mm, and 20 mm diameter bars to evaluate stress–slip responses, bond efficiency, and bond energy absorption. The results demonstrated that SCC consistently outperformed NC, achieving peak bond stresses that were 12–28% higher, depending on bar size and mix proportions. In addition, SCC specimens exhibited up to 35% greater bond energy absorption, reflecting improved toughness and enhanced slip mobilization. The findings also confirmed that compressive strength alone cannot reliably predict bond capacity; instead, factors such as bar diameter, rib geometry, and concrete rheology exert a more significant influence. Overall, the study provides the first detailed evidence of how reinforcing steel bars recycled from scrap metals interacts with SCC, highlighting its potential for durable and resilient construction.

**Keywords:** Local bond, slip, self-compacting concrete (SCC), recycled scrap metal, reinforcing steel bar, reinforced concrete durability, sustainable construction

## 1. Introduction

The bond between reinforcing steel and surrounding concrete is a central mechanism that governs the composite action of reinforced concrete members. Effective bond ensures stress transfer across the steel–concrete interface, contributing to load resistance, crack control, ductility, and long-term durability. Traditionally, bond performance has been studied through pull-out or beam-end tests, with earlier works by Tepfers (1979) [38], Orangun *et al*. (1977) [33], and Darwin *et al*. (1996) [16] establishing fundamental relationships between concrete strength, bar geometry, and anchorage capacity. These studies highlighted the contribution of adhesion, friction, and mechanical interlock to bond development, particularly in deformed bars. However, subsequent research has demonstrated that compressive strength alone is not a reliable predictor of bond, as microcracking, stiffness, and concrete heterogeneity often alter local bond-slip responses (Esfahani & Rangan, 1998) [21].

The advent of self-compacting concrete (SCC) has further reshaped the discourse on bond behavior. Owing to its superior flowability and self-consolidation, SCC often enhances the interfacial contact between concrete and reinforcement, leading to higher peak bond stresses. Yet, findings remain mixed regarding post-peak behavior. Several recent studies confirm that SCC can produce either

brittle, stiff bond-slip responses with limited deformation capacity or, under optimized conditions, highly ductile behavior with significant bond energy absorption (Shunmuga Vembu *et al*., 2023) [37]. This duality underscores the importance of mix design and rheological balance in determining bond performance.

Recent research has also placed stronger emphasis on the role of bar size, rib geometry, and surface characteristics in shaping local bond mechanisms. Large-diameter bars often demonstrate reduced bond efficiency due to lower surface-to-volume ratios and higher splitting stresses, whereas smaller diameters promote uniform stress distribution and stable post-peak slip (Harajli *et al*., 1995; Biscaia *et al*., 2023) [24, 8]. The influence of rib geometry is particularly critical in contexts such as Ghana, where locally milled reinforcement from scrap metals may deviate significantly from international production standards (Kankam, 2004) [29]. Surface irregularities and rib variability as found in some locally manufactured bars from scrap metal in Ghana directly affect mechanical interlock, necessitating empirical bond-slip data for regionally manufactured steels. (Kankam *et al*., 2023; Quarm Junior *et al*., 2024; Banini *et al*. 2022) [30, 34, 7].

Methodologically, the field of bond tests in reinforced concrete has advanced with the introduction of cyclic and push-off bond tests, which better simulate in-service and seismic loading conditions (Domingues *et al*., 2010; Biscaia *et al*., 2023) [17, 18, 8]. Finite-element and discrete models now embed calibrated bond-slip laws, improving translation of pull-out data into member-level predictions (Corres, 2024) [15]. Another significant trend is the use of bond energy absorption metrics derived from the area under bond stress–slip curves, a measure that reflects bond toughness and provides deeper insight into ductility and fracture bond energy at the interface (Biscaia *et al*., 2023) [8].

Despite these advances, most international bond models are calibrated using commercially standardized reinforcing steel bars and may not be directly applicable to locally produced bars in developing economies. Furthermore, comparative studies of SCC and normal concrete (NC) under identical conditions remain limited, especially with multiple bar diameters and locally sourced steel. Finally, while compressive strength continues to dominate design practice, there is increasing recognition that deformation capacity, slip mobilization, and bond energy absorption provide more reliable measures of structural resilience, particularly under seismic or cyclic loading.

Against this backdrop, the present study investigates the local bond-slip behavior of Ghanaian-manufactured steel bars from scrap metal that are embedded in SCC and NC. By combining double pull-out testing with detailed analysis of bar size, concrete strength, and bond energy absorption, this work contributes context-specific evidence to guide both structural design codes and sustainable material on the strength and deformation of concrete members.

## 2. Materials and Methods

**2.1 Materials:** The concrete mix comprised ordinary Portland cement which satisfied the requirement of BS 12:1991; river sand as fine aggregate; crushed granite as coarse aggregate (12mm); and potable water. In addition, a superplasticizer (MC-Power flow 6425) was added to the concrete to produce self-compacting concrete.

### 2.1.1 Superplasticizer

Superplasticizers are an essential component of modern concrete since they improve workability at low water-to-cement levels, allowing the production of long-lasting and environmentally friendly concrete. Superplasticizers are high-range water reducers that comply with ASTM C 1017 and are used in concrete to provide high-slump streaming concrete with a low-to-normal slump and water-cement ratio. Flowing concrete is a fluid and workable concrete that requires minimal to no vibration to compress and is generally free of bleeding and segregation. The type of superplasticizer used for this research was MC-Power flow 6425.

### 2.2 Sieve Analysis

Tests of particle size distribution of the aggregates and silt content in fine aggregates were conducted per BS 812 Part 103 (1985) and the results are shown in Figure 1a and 1b;

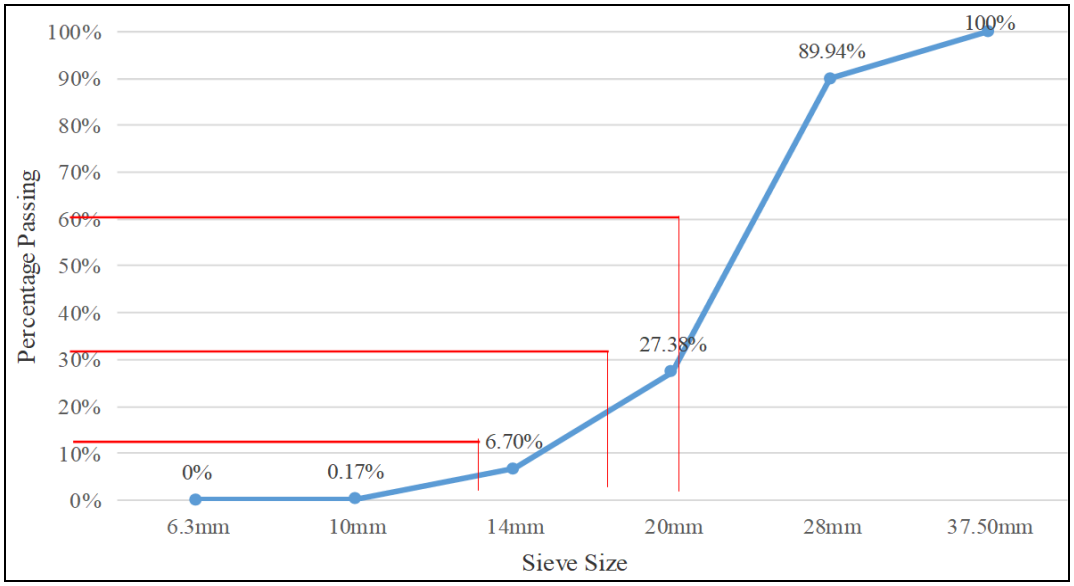


**Fig 1a:** Particle size distribution curve of coarse aggregate (virgin)

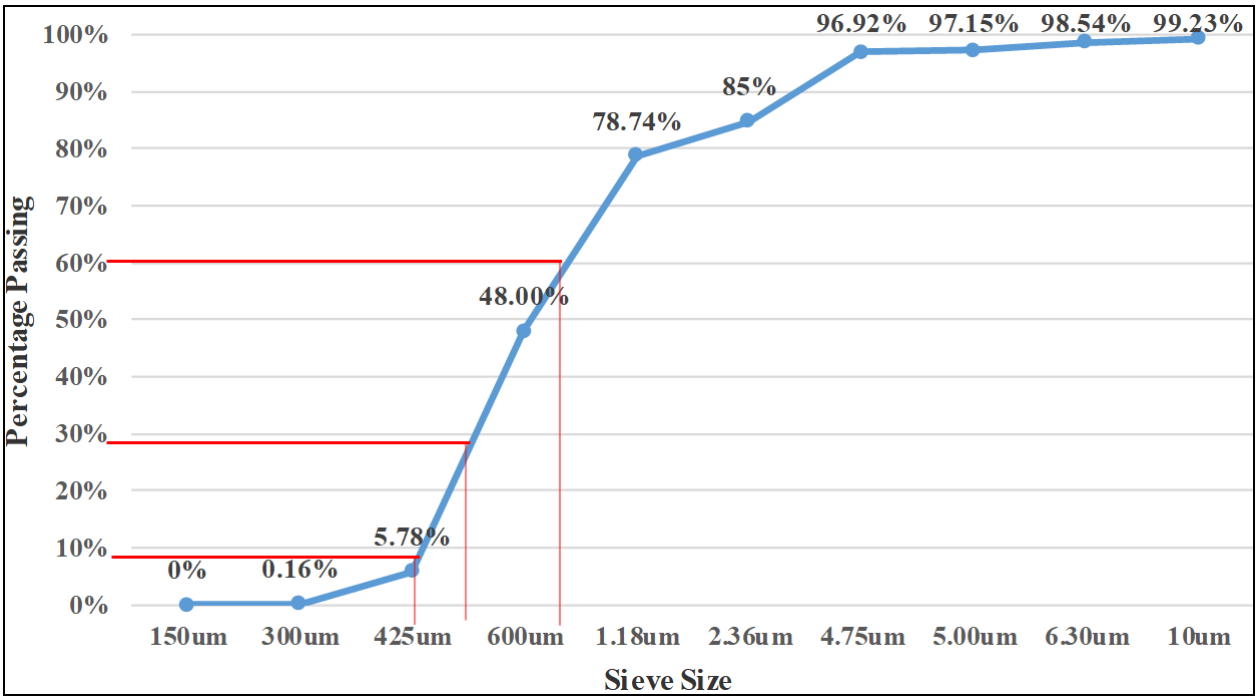


**Fig 1b:** Particle size distribution curve of sieve fine aggregates.

### 2.3 Design of test specimens

Tables 1 present the details of test specimens for different mixes as outlined in the following:

NC1 /NC2 – cement, sand, gravel with 0.55 water cement ratio

SCC1 / SCC2 – cement, sand, gravel 0.28 water cement ratio and 1.4% superplasticizer.

Test results of the concrete mixes are shown in table 1;

**Table 1:** Details of Concrete Mixes.

| Compressive Strength Test Results | | | | |
|---|---|---|---|---|
| **Type of concrete** | **Age** | **Density (Kg/m³)** | **Compressive strength (N/mm²)** | **Tensile Strength (N/mm²)** |
| (MIX 1– 1:2:4, w/c ratio 0.55 & 1:3.5:2.5 w/c ratio=0.28 with 1.4% Superplasticizer) | | | | |
| Normal Concrete Mix 1- (NC1) | 7 days | 2075.36 | 15.59 | 1.89 |
| SCC Mix 1- (SCC1) | | 2424.9 | 30.00 | 3.25 |
| (MIX 2 – 1:1.5:3, w/c ratio=0.55 & 1:2.75:1.75, w/c ratio=0.28 with 1.4 Suplasticizer) | | | | |
| Normal Concrete Mix 2- (NC2) | 7 days | 2902.97 | 19.1 | 3.33 |
| SCC Mix 2 (SCC 2) | | 3012.54 | 33.21 | 5.96 |
| (MIX 1 – 1:2:4, w/c ratio 0.55 & 1:3.5:2.5 w/c ratio=0.28 with 1.4% Superplasticizer) | | | | |
| Normal Concrete- Type 1 (NC1) | 21 Days | 2255.86 | 17.02 | 2.16 |
| SCC Mix 1 (SCC 1) | | 2187.73 | 33.84 | 3.9 |
| (MIX 2 – 1:1.5:3, w/c ratio=0.55 & 1:2.75:1.75, w/c ratio=0.28 with 1.4 Suplasticizer) | | | | |
| Normal Concrete- Type 2 (NC2) | 21 Days | 2349.82 | 22.97 | 5.24 |
| SCC Mix 2 (SCC2) | | 2495.82 | 36.79 | 7.88 |
| (MIX 1 – 1:2:4, w/c ratio 0.55 & 1:3.5:2.5 w/c ratio=0.28 with 1.4% Superplasticizer) | | | | |
| Normal Concrete - (NC1) | 28 Days | 2319.18 | 24.28 | 2.97 |
| SCC Mix 1 – (SCC1) | | 2380.68 | 34.93 | 5.91 |
| (MIX 2 – 1:1.5:3, w/c ratio=0.55 & 1:2.75:1.75, w/c ratio=0.28 with 1.4 Suplasticizer) | | | | |
| Normal Concrete- Type 2 (NC2) | 28 Days | 2372.05 | 28.15 | 6.11 |
| SCC Mix 2 – (SCC2) | | 2854.35 | 38.88 | 9.21 |

### 2.4 Slip Measuring Instrument

The slip of the bar was measured by means of a device that consisted of a cylindrical steel tube to which a pair of dial gauges were attached on opposite sides by a steel stud on the back of each gauge (Fig.2a and 2b). The steel stud fitted into a hole drilled in the wall of the tube and was secured by a set-screw. The tube fitted over the end of the reinforcing bar where the latter projected from the concrete and was secured to it approximately 12mm from the face of the concrete by means of three screws through the tube wall, which gripped the bar by bearing on it in a radial direction. The plungers of the dial gauges were then in contact with the face of the concrete 27mm from the center of the bar. The internal diameter of the tube was 28mm. The same tube was used on the 20mm test bars, but a second tube 18mm in internal diameter was used for the 16mm bars where the plungers of the dial gauges were in contact with the face of the concrete 24mm from the center of the bar relative to the surrounding concrete. The latter, measured by means of dial gauges was corrected for the extension of the small length of free bar between the concrete face and the reference point in the bar.

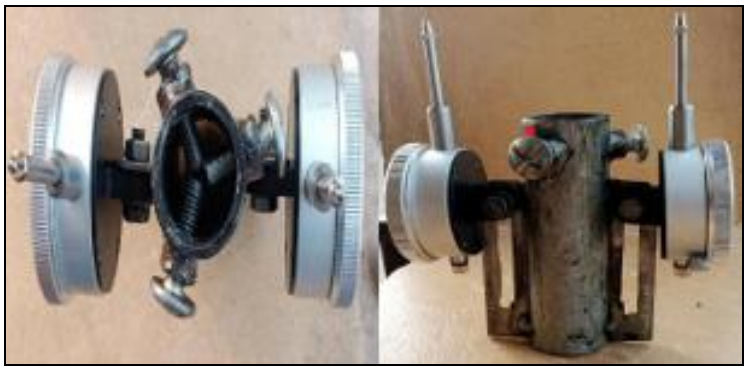

**Fig 2a:** Picture of slip measuring Device

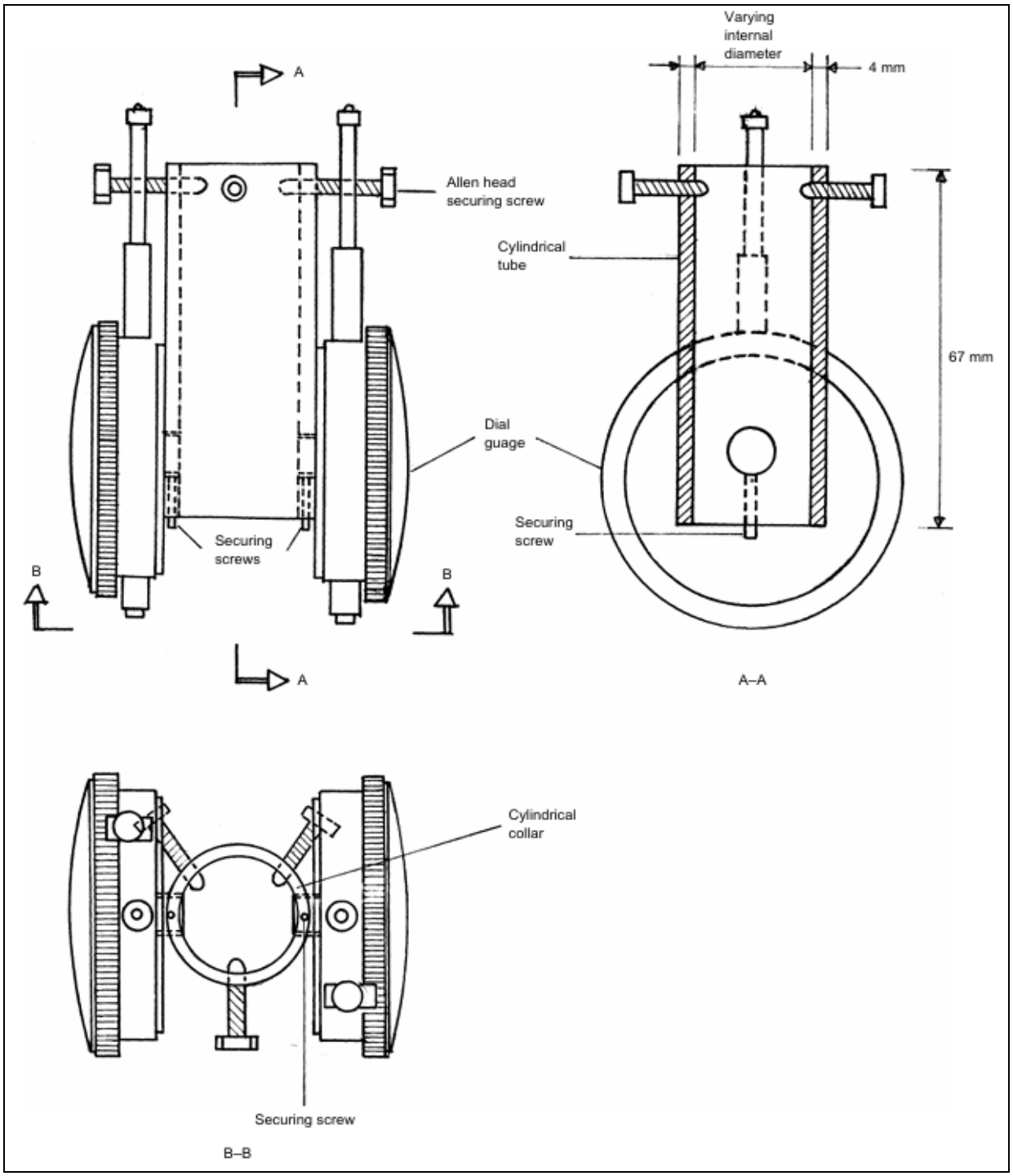


**Fig 2b:** Details of slip measuring Device

### 2.5 Mixing

#### 2.5.1 Batching of the Materials

Weight-based batches were prepared for fine and coarse aggregates, cement, and water in accordance with ASTM C192/C192M-19; SCC fresh-state targets and procedures followed EFNARC (2002) [20]. The superplasticizer was measured by volume with respect to the cement.

#### 2.5.2 Concrete mix design

Two different mixes with equal cement to aggregate ratios were deployed for both the self-compacting concrete and normal control concrete with the objective of studying the local bond stress of the reinforcing steel bars embedded in the concrete mixes. The concrete mixes were 1: 2: 4 (1:6) and 1: 1.5: 3 (1:4.5) with 0.55 water cement ratio for the Normal Conventional concrete and its SCC counterparts with low water cement ratio of 0.28 and 1.4% added superplasticizer being 1:3.5:2.5 (1:6) and 1:2.75:1.75 (1:4.5) as shown in table 1. The low water cement ratio aided the SCC to achieve higher compressive strength and the added 1.4% superplasticizer with the flow and other matching properties.

#### 2.5.3 Mixing and curing of specimens

Mixing of the concrete was done mechanically in a concrete mixer. The proportions of fine aggregates and cement were first batched into the concrete mixer, followed by the coarse aggregates. Mixing of the constituent materials was done in the dry state for about two minutes, and then batched water was progressively added to the dry mixed materials in the mixer. Mixing was standardized and had a consistent hue in a plastic mix. For thorough mixing, the time for blending was 1.5 to 2 minutes per rotation. A slump test was conducted to determine the workability of the concrete. 24 concrete cubes measuring 150mm x 150mm x 150mm, and 24 cylinders measuring 150mm diameter by 300mm height, were cast to study the compressive strength, split tensile. The bond specimen consisted of 42 double pull-out specimens of both SCC and NC concrete mixes. Concrete for each test specimen was cast in three layers and each layer was compacted by tampering 25 strokes using a rod. Curing of the local bond specimen, cubes, and cylinders was by fully covering the specimens with wet sacks to obtain a temperature equivalent to ambient average laboratory temperature of 28 ºC and 100 percent relative humidity to avoid micro–cracking of the test specimens. The cube specimens that were designated were tested at seven, fourteen, and twenty-eight days of age; the Local Bond specimens were tested at age twenty-eight days.

#### 2.5.4 Test procedure

The pull-out tests were carried out in an Avery Denison universal testing machine with a cross-head speed of 0:51mm per min in a room controlled at 19 ºC and 65% relative humidity. The load was applied incrementally to each free end of the bar to the maximum corresponding to the maximum working stress of therein forcing bar (service strength 140N/mm$^2$ and 250N/mm$^2$; yield strength 250N/mm$^2$ and 420N/mm$^2$ respectively), Each load increment was followed by measurement of the overall elongation of the bar relative to the surrounding concrete. The latter, measured by means of dial gauges was corrected for the extension of the small length of free bar between the concrete face and the reference point in the bar.

### 2.6 Bond Energy

Bond energy is the work done to break bond between reinforcing steel bar and concrete through slip. To calculate the bond energy absorbed by the bond between steel and concrete in the specimen, the bond stress-slip curve is integrated numerically. This bond energy represents the area under the bond stress vs slip curve, which is crucial in bond behavior because it characterizes the toughness or ductility of the bond interface. To determine the bond energy per unit bonded area (N/mm²) absorbed during the pull-out test, the area under the bond stress-slip curve is calculated.

#### 2.6.1 Computation of Bond Energy absorbed by Trapezoidal Integration

The trapezoidal numerical integration of bond stress (τ) over slip (s):

$$E = \int \tau \, ds \approx \sum_{i=1}^{n-1} \frac{(\tau_i + \tau_{i+1})}{2} \cdot (s_{i+1} - s_i)$$

Where:
Bond Energy absorbed (N/mm)
*Ti* = Bond stress at point *i* (Nmm$^2$)
*Si* = slip at point *i (mm)*

The bond energy per unit bonded area gives a quantifiable measure of the bond toughness or fracture bond energy of the steel-concrete interface for this specimen. High bond energy values reflect strong mechanical interlock, effective stress transfer, and more ductile behavior before failure compared to other specimen, this value can show how local materials and mix designs affect bond performance.

### 2.7 Experimental Methods

#### 2.7.1 Preparation of double pull-out bond specimen

The steel bars were cut into 120 pieces of length 620mm, and pretreated in conformity with ASTM A 775/A 775M – 01, by cleaning with metal brush and thinner to remove dirt, grease/oil substance and metal oxide from the surface of the steel bar. They were then cleaned with potable water, wiped with cotton rag and dried. The centers were drilled to receive tight transverse 75mm anchor bars to serve as the reference point of the stress and slip that would occur during the double pull-out test and represent point midway between two adjacent cracks in a beam.
This stage was followed by fixing the rebars in pre-lubricated mold box in order to cast the bond prism specimens. Concrete mix ratios: (NC: 1:2:4 1:1.5:3 with water cement ratio 0.55 and SCC: 1:2.75:1.75/1:3.5:2.5 w/c ratio=0.28 with 1.4% Superplasticizer) was prepared from the above materials using a mechanical concrete mixer for consistency. They were then cleaned and sent to the laboratory after 28 days for various tests.

### 2.8 Double pull-out Test

The double pull-out test was conducted on the bond

specimens using a universal machine (Avery-Denison's classic 500kN T-series - T42B/C model). Other tools and instruments involved were 4 dial-gauges, camera, slip measuring instrument which comprised dial gauge to the rebar before testing. Each specimen had two projected rebars fit into the upper and lower grip of the universal machine after fixing the dial gauges. Loading was done incrementally at 2kN intervals to measure the local bond at each load increment. The 16mm high yield specimens were loaded at 5kN interval due to the high service stress at the rebar. The loading was done such that both the rebar and the concrete were in tension. The loading, irrespective of interval was at the rate of 1mm/min or 0.5kN/s (ASTM A944). A pair of two dial gauge readings were taken at the top while another pair at the bottom. The average reading of the two readings in each case was used for analysis of slip. This was meant to reduce error level if just one gauge is used.

The specimens were tested within the service limit of the particular rebar-12mm or 16mm, high yield steel or mild steel rebar. The service limit was calculated based on the strength (140N/mm$^2$ and 250N/mm$^2$ for mild and high yield steel respectively) and the actual cross-sectional area of the rebars. Hence, the local bond maximum pull-out load for the various rebars were 15kN, 26kN, 36kN and 65kN for 12mm mild steel, 16mm mild steel, 12mm high yield steel and 16mm high steel respectively. Fig.6 shows the set-up for the bond test.

## 3. Analysis of Results

The results were illustrated graphically by presenting the bond stress–slip relationship curves and statistically analyzed using Microsoft Excel on the computed bond stress and slip values of the test specimens.

### 3.1 Local Bond Test

A prismatic double pull-out specimen (150mm X 150mm X 200 mm) that had a transverse anchor bar at the center of the reinforcement to predetermine the point which is not zero but slip halfway between two cracks was selected to simulate the actual loading of reinforcement between cracks in a structural concrete member. A 200 mm length of embedment was chosen to represent a crack spacing that was long enough to allow a satisfactory variation of stress in the reinforcing bar and short enough to avoid the formation of a transverse crack in the concrete. The test specimen is shown in Fig. 3;

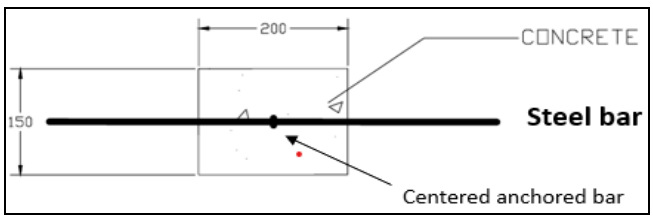


**Fig 3:** Double pull-out bond specimen.

## 4. Results and Discussion

### 4.1 Bond Stress

Bond Stress in reinforced concrete refers to the interactive mechanism that enables the effective transfer of stress between reinforcing steel bars and the surrounding concrete matrix. This interaction is fundamental to the composite action of reinforced concrete members and is essential for ensuring the structural integrity, crack control, and load-carrying capacity of reinforced concrete elements. The bond stress mechanism is governed by a combination of adhesion, friction, and mechanical interlock, particularly in deformed bars, which are standard in modern construction.

Bond stress behavior is typically categorized into two interrelated but distinct components: local bond and anchorage bond. Each plays a specific role in structural performance and is influenced by various factors such as bar diameter, surface texture, concrete strength, and confinement conditions.

### 4.2 Analysis of Local Bond Stress

The local bond was determined using the bar slip data and the position along the reinforcement bar, applying the three-dimensional equations (bond stress – steel stress – slip) developed by Kankam (1997, 2003) [26, 27]. These equations were used to calculate the average bond stress along the embedded length of the rebar in concrete for each slip value, starting from the transverse anchor point (representing the midpoint between two adjacent cracks in a beam) to the loaded end of the concrete (representing the crack face). The three equations presented as Equations 1 to 3 were specifically formulated for plain mild steel, cold-worked steel, and hot-rolled steel rebars, respectively (Kankam, 1997, 2008) [26, 28].

1. Plain round bar: $f_b = (41.7 – 0.2f_s)\ \Delta^{0(8}$ …… Eq. (1)
2. Cold worked bar: $f_b = (55 – 0.5x)\ \Delta^{0.5}$ …… Eq. (2)
3. Hot rolled bar: $f_b = (35 – 0.3x)\ \Delta^{0.5}$ …….. Eq. (3)

**Where,**

fb represents the bond stress (in N/mm²),
x is the distance from the center of the embedded length (in mm),
fs is the steel stress, and
Δ is the total slip of the embedded bar.

The constant 35 and the coefficient 0.3 are influenced by factors such as the diameter of the rebar, the strength of the concrete, the type of loading applied, and the surface characteristics of the reinforcement bars (Kankam, 1997, 2003) [26, 27].

The calculation of average bond stress was carried out by selecting two specific points along the embedded length of the rebar. In this study, the formula developed for hot-rolled steel bars was used, as the test specimens were reinforced with hot-rolled deformed rebars. This specific formula, with defined parameters, is presented in Equation 3.

To determine the average bond stress between the start of the embedment (x = x2 = 100 mm) and the central (anchored) point of the embedment (x = x1 = 0 mm) for a given total measured slip, Equation 4 derived from Equation 3 was used.

$f_b = [(35 - 0.3x_1)\ \Delta^{0.5} + (35 - 0.3x_2)\ \Delta^{0.5}]/2$ ……Eq. (4)

$X_1 = 0$ (from centre of embedment)

$X_2 = 100$ (from centre of embedment to face where the rebar enters the specimen [crack face])

Δ = slip (mm).

The graphs and pictures of local bond-stress and Slip shown below;

a: Prepared rebar specimens b: Slump Test for Self-compacting concrete c: Bond specimen mold box

**Fig 4:** Rebar preparation, coating and geometry information processes.


a: Bond test setup b: Bond test setup

c: Dial gauges fixed the specimen d: Bond specimens stacked after testing

**Fig 5:** Bond specimen testing setup.

### 4.3 Relationship of local bond stress versus Slip

#### 4.3.1 Influence of bar size in NC and SCC Mixes

##### 4.3.1.1 R12 Bar Series

For the smallest diameter bars (R12), the NC mixes revealed two contrasting behaviors. At the lower concrete strength R12-NC1, bond strength was moderate (3.12 N/mm²) but the slip was minimal (0.08 mm), and 0.13 N/mm bond energy, resulting in a stiff bond–slip response that failed abruptly. Conversely, at higher strength R12-NC2, bond strength reduced slightly to 2.62 N/mm², but slip increased dramatically to 2.23 mm, and 3.09 N/mm bond energy producing a markedly post-peak performance and the highest bond energy absorption in the R12 set (3.09 N/mm).

When SCC was introduced, the R12-SCC1 specimen attained the highest bond stress in the series (3.836 N/mm²) with very low slip (0.14 mm), and 0.38 N/mm bond energy indicating a strong but brittle anchorage. However, at the highest SCC strength R12-SCC2, bond capacity reduced to 2.99 N/mm² with only 0.11 mm slip, and a bond energy of 0.252 N/mm showing both strength and deformation losses, possibly due to reduced mechanical interlock from the smooth SCC matrix.

##### 4.3.1.2 T12 Bar Series

The T12 bars displayed more consistent performance in NC mixes. Both T12-NC1 and T12-NC2 recorded bond strengths above 3.60 N/mm² with slips in the range of 0.816–0.857 mm, and bond energy range of 2.60 N/mm – 2.54 N/mm, resulting in balanced strength–deformation profiles and stable post-peak behavior.

In SCC mixes, performance shifted. While the T12-SCC1 specimen retained high peak bond (3.607 N/mm²), its slip reduced to 0.402 mm, halving the bond energy absorbed compared to NCC, signaling a stiffer and more abrupt

failure. SCC2 achieved the highest bond in the T12 set (3.909 N/mm²) but again showed limited slip (0.47 mm) and bond energy (1.08 N/mm), indicating that stiffness, rather than deformation, dominating its behavior.

#### 4.3.1.3 T16 Bar Series

The T16 series provided the most outstanding deformational differences. In NC mixes, bond strength improved from 3.596 N/mm² at T16-NC1 to 3.95 N/mm² at T16-NC2, accompanied by a near doubling of slip (0.53 mm to 1.00 mm). This produced a desirable combination of high strength and good bond-slip strength within the concrete.

SCC mixes introduced a dramatic shift. At T16-SCC1 having a bond strength of 3.60 N/mm$^2$, slip increased to 4.77 mm with an energy absorption of 13.14 N·mm which is the highest in the entire dataset clearly indicating an exceptionally bond–slip relationship. However, at T16-SCC2 recording a bond strength of 3.49 N/mm$^2$, despite a reasonable slip (1.75 mm), the bond energy dropped sharply to 0.65 N/mm, suggesting a premature bond decrease and reduced post-peak load retention.

#### 4.3.1.4 T20 Bar Series

For the largest bars, NC mixes at both T20-NC1 and T20-NC2 showed moderate bond strengths (3.33–3.422 N/mm²) and slips of 0.742–1.00 mm, and bond energy of 2.09 N/mm – 1.87 N/mm producing stable bond–slip responses with good bond strength.

In SCC mixes, bond capacity dropped slightly (3.120 N/mm² at T20-SCC1) and having producing a bond energy of 1.67 N.mm but bond-slip strength remained moderate (0.808 mm slip). The T20-SCC2 specimen recorded the lowest bond in the series (2.69 N/mm²) despite reasonable slip (0.902 mm) and 1.82 N/mm bond energy, suggesting that the SCC's smooth paste may not provide sufficient local bond strength for large-diameter bars.

**Table 2:** Details of Local Bond Specimen

| Specimen Id | Local bond Stress (N/Mm$^2$) | Maximum Slip (Mm) | Bond Energy Absorbed (N/mm) | Remarks |
|---|---|---|---|---|
| R12-NC1 | 3.12 | 0.08 | 0.13 | Very stiff response with minimal slip before peak; brittle bond failure |
| R12-NC2 | 2.62 | 2.23 | 3.09 | Moderate bond strength but large slip; ductile post-peak behavior. |
| R12-SCC1 | 3.836 | 0.14 | 0.38 | High bond strength with limited slip |
| R12-SCC2 | 2.99 | 0.11 | 0.252 | Lower bond with minimal slip |
| T12-NC1 | 3.607 | 0.857 | 2.60 | Strong bond with moderate slip; balanced strength–ductility profile. |
| T12- NC2 | 3.685 | 0.816 | 2.54 | Similar to previous, consistent mechanical performance. |
| T12-SCC1 | 3.607 | 0.402 | 1.08 | Strong initial bond but lower bond energy; abrupt post-peak decay. |
| T12--SCC2 | 3.909 | 0.47 | 1.08 | High peak bond, limited energy; stiffness dominates behavior |
| T16-NC1 | 3.596 | 0.53 | 1.26 | Good strength with moderate slip; cohesive bond characteristics. |
| T16-NC2 | 3.95 | 1 | 2.86 | High bond with good slip capacity; favorable ductile performance. |
| T16-SCC1 | 3.60 | 4.77 | 13.14 | Exceptional slip and bond energy absorption; highly ductile anchorage. |
| T16-SCC2 | 3.49 | 1.75 | 0.65 | Moderate slip but low bond energy; suggests early bond degradation. |
| T20-NC1 | 3.33 | 0.742 | 2.09 | Balanced bond and slip and stable bond–slip response. |
| T20-NC2 | 3.422 | 1 | 1.87 | Good ductility with steady bond retention. |
| T20-SCC1 | 3.120 | 0.808 | 1.67 | Lower bond but moderate ductility retained. |
| T20-SCC2 | 2.69 | 0.902 | 1.82 | Lowest bond |

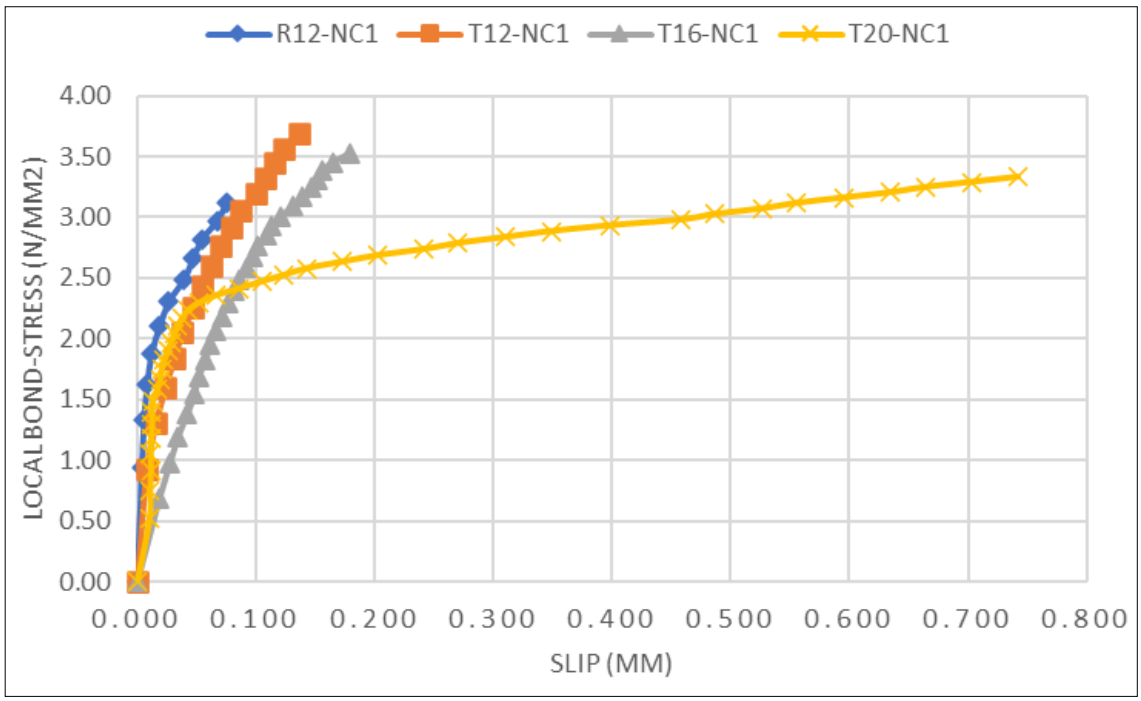


**Fig 6:** Local bond-stress/slip of bar sizes (R12, T12, T16, T20) in concrete mix (NC1)

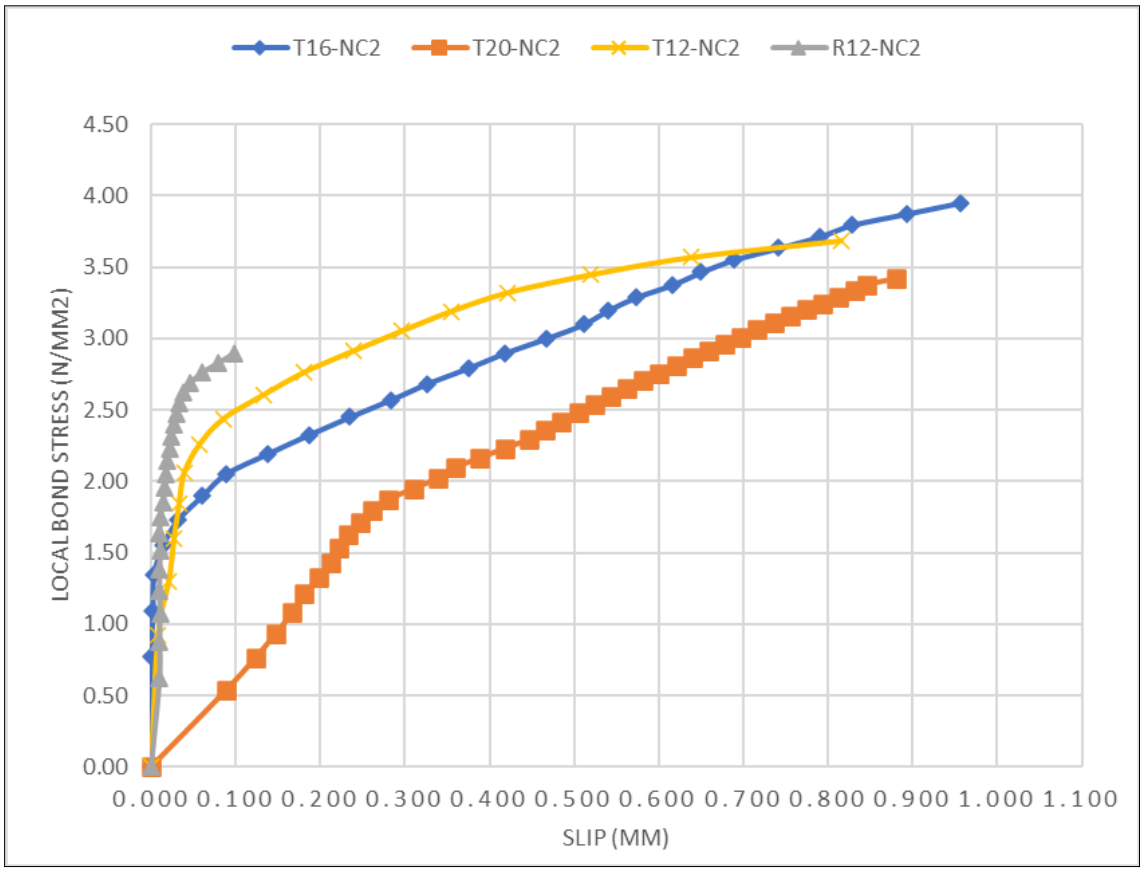


**Fig 7:** Local bond-stress/Slip of bars (R12 T12, T16, T20) in concrete mix (NC2).

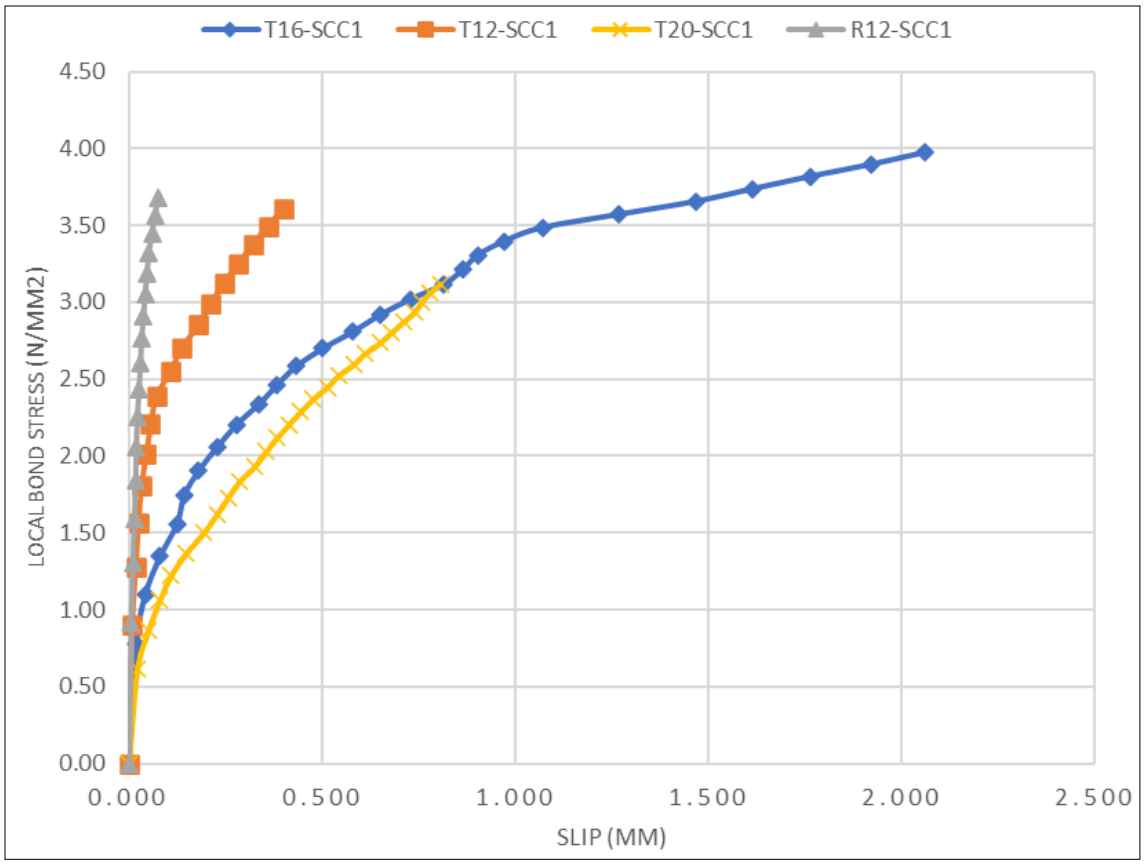


**Fig 8:** Local bond-stress/Slip of bar sizes (R12, T12, T16, T20) in Concrete mix (SCC1).

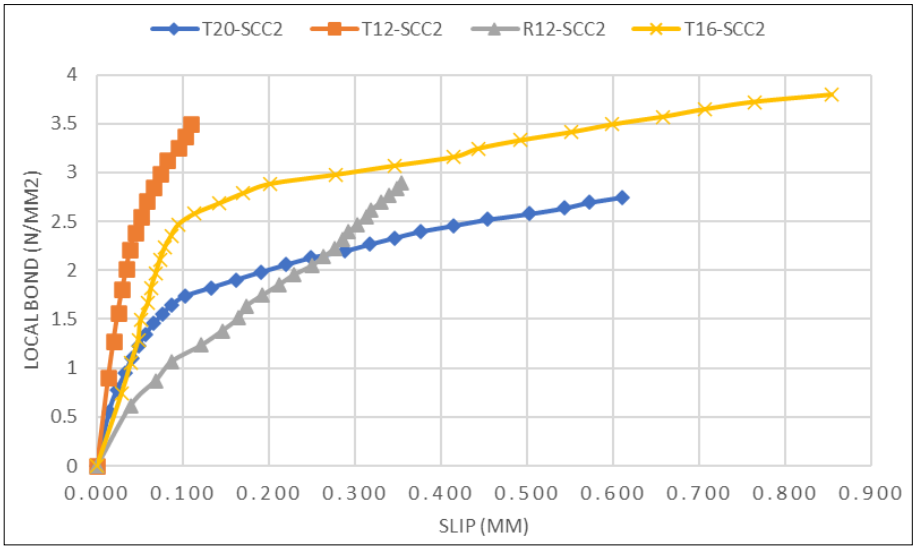


**Fig 9:** Local bond-stress/Slip of bar sizes (R12, T12, T16, T20) in concrete mixes (R12, T12, T16, T20) in concrete mix (SCC2).

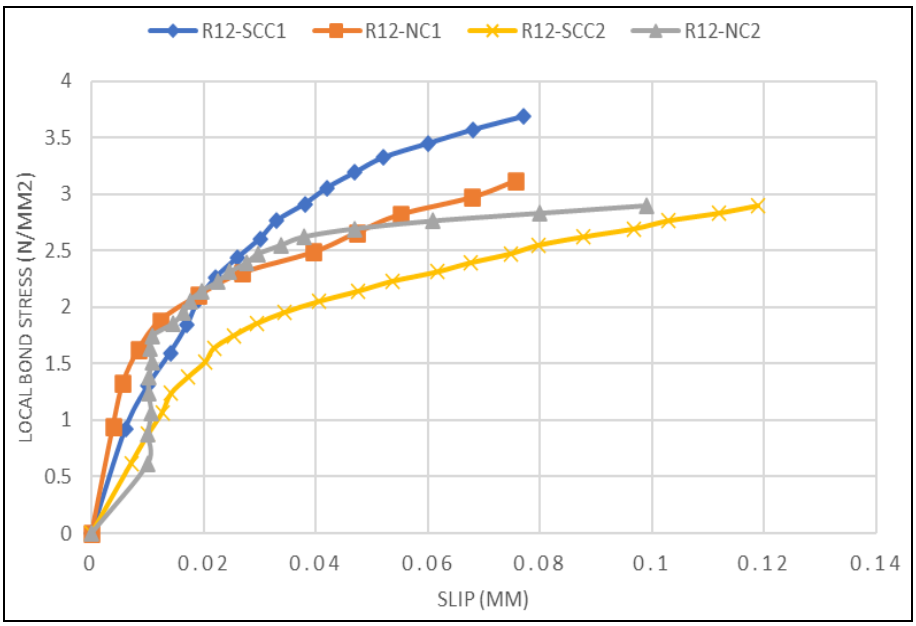


**Fig 10:** Local bond-stress/Slip of bar size (R12mm) in concrete mixes (NC1, NC2, SCC1, SCC2).

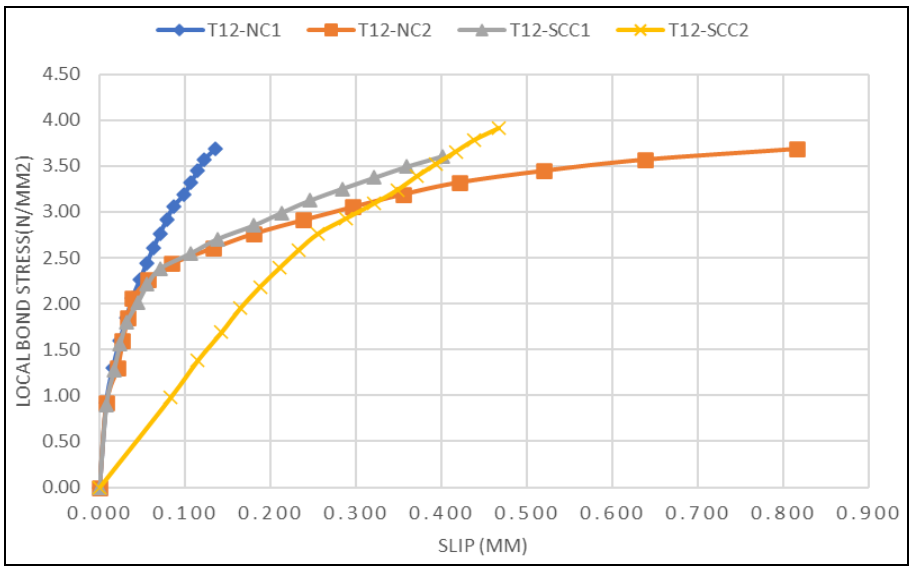


**Fig 11:** Local bond-stress/Slip of bar size (T12mm) in concrete mixes (NC1, NC2, SCC1, SCC2).

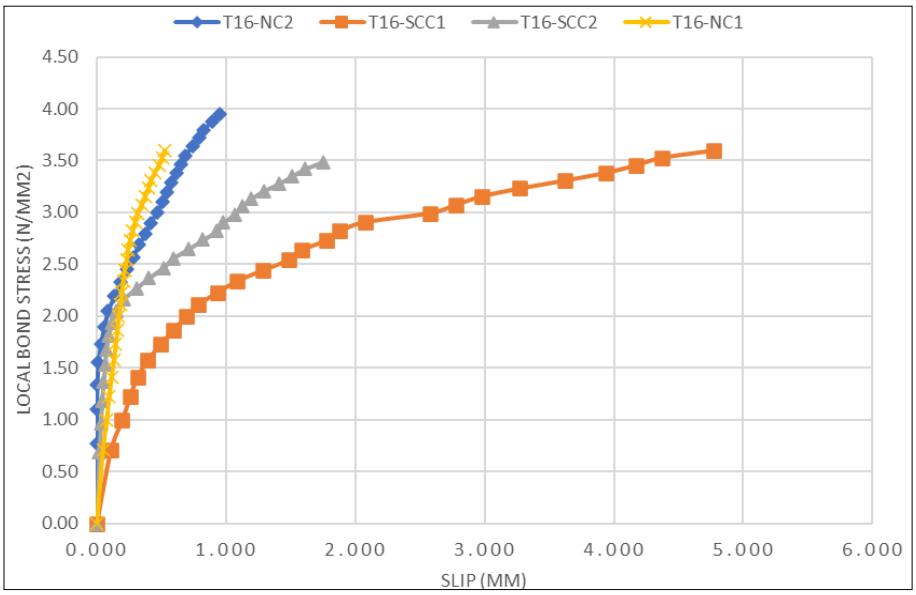


**Fig 12:** Local bond-stress/Slip of bar size (T16mm) in concrete mixes (NC1, NC2, SCC1, SCC2).

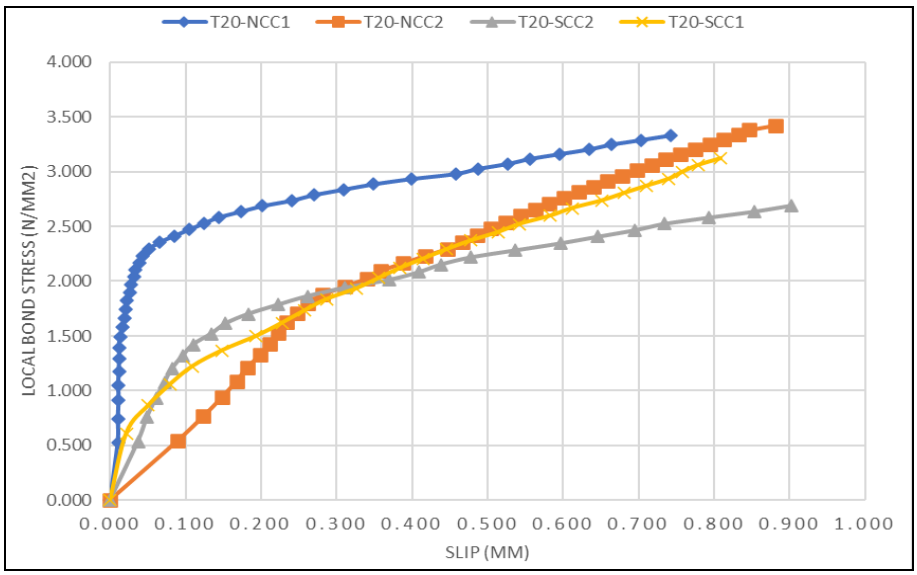


**Fig 13:** Local bond-stress/Slip of bar size (T20mm) of bars in concrete mixes (NC1, NC2, SCC1, SCC2).

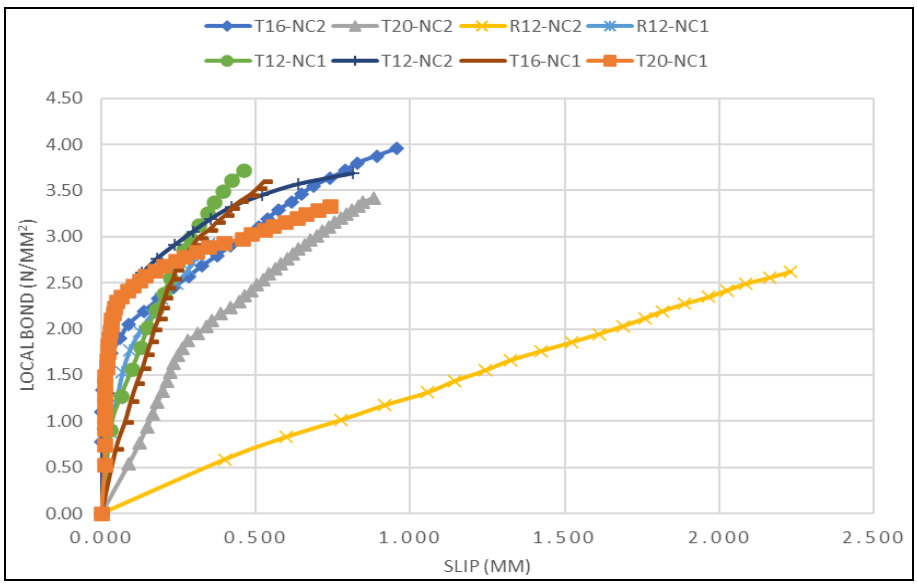


**Fig 14:** Local bond-stress/Slip of bar sizes (R12, T12, T16, T20) in concrete mixes (NC1, NC2).

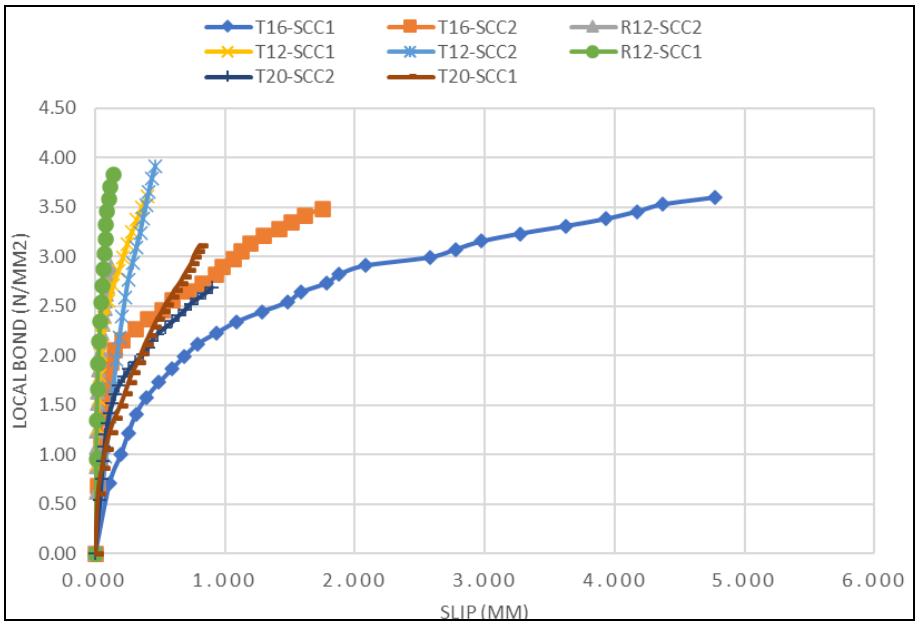


**Fig 15:** Local bond-stress/Slip of bar sizes (R12, T12, T16, T20) in concrete mixes (SCC1 SCC2).

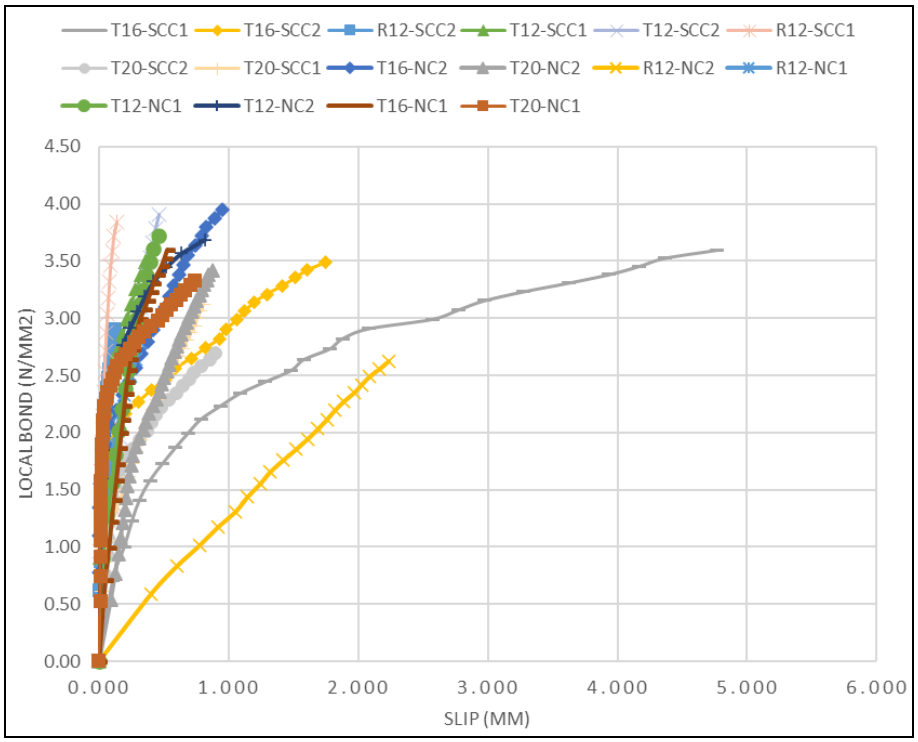


**Fig 16:** Local bond-stress/Slip of bar sizes (R12, T12, T16, T20) in concrete mixes (NC1, NC2, SCC1, SCC2).

### 4.3.2 Influence of Concrete Strength

The R12-NC1 specimen recorded a peak bond of 3.12 N/mm² with minimal slip (0.08 mm) and (0.13 N/mm) bond energy, resulting in a brittle bond failure, whereas the higher-strength R12- NC2 achieved only 2.62 N/mm² but exhibited far greater slip (2.23 mm) and significantly higher bond energy absorption (3.09 N/mm). A consistent trend emerges in which increases in concrete compressive strength do not always lead to proportional gains in bond strength, a finding consistent with earlier observations by Tepfers (1979) [38] and Orangun *et al.* (1977) [33]. This suggests that, beyond a certain strength level, microcracking at the steel–concrete interface and the brittleness of the matrix may offset the expected increases in peak bond.

SCC specimens displayed a slightly different response. R12-SCC1 achieved the highest bond strength in the R12 series (3.836 N/mm²) with low slip (0.14 mm), indicating strong interfacial adhesion. However, the R12-SCC2 showed reduced bond strength (2.99 N/mm²) despite higher compressive strength, reinforcing the idea that excessive stiffness in high-strength SCC can lead to premature bond deterioration, in line with findings by Esfahani and Rangan (1998) [21].

SCC specimens exhibited steeper ascending branches, indicating stronger initial adhesion and interlock. However, post-peak responses varied by bar size.

1. 12 mm bars (SCC): Showed ductile slip mobilization with sustained residual bond capacity, ideal for energy dissipation in seismic conditions.
2. 20 mm bars (SCC): Displayed sharper post-peak declines, reflecting reduced bond efficiency at larger diameters, consistent with findings by Harajli *et al.* (1995) [24].

This behavior underscores the influence of bar diameter and rib geometry, confirming that compressive strength alone cannot predict slip response, in agreement with recent international reviews (Shunmuga Vembu *et al.*, 2023) [37].

### 4.3.3 Influence of Bar Size on Local Bond Performance

Bar diameter exerted a notable influence on bond behavior. The T12 bars, in both NC and SCC, demonstrated balanced bond strength–slip capacity performance, with peak bonds in the range of 3.60–3.91 N/mm² and moderate slips (0.40–0.86 mm). These results support Darwin *et al.* (1996) [16], who observed that smaller bar diameters tend to engage more effectively with the surrounding matrix, promoting a uniform bond stress distribution.

In contrast, the T16 series highlighted one of the most remarkable differences between NC and SCC. While T16-NCC2 displayed high bond (3.95 N/mm²) and favorable slip capacity of (1.00 mm slip, and 2.86 N/mm bond energy absorption), the T16-SCC1 showed exceptional slip (4.77 mm) and an extraordinary bond energy absorption of 13.14 N/mm which by far is the highest recorded. This indicates that SCC, when optimally proportioned, its local bond exhibited can develop favorable slip capacity with superior bond energy dissipation, a response that may enhance performance in seismic-resistant design.

The T20-NC1 specimen achieved a stable performance (3.33 N/mm², 0.742 mm slip), while the T20-SCC2 also recorded the lowest bond of the series (2.69 N/mm²) for the largest bars tested, both NC and SCC of T20 exhibited lower peak bonds compared to smaller diameters, in agreement with Harajli *et al.* (1995) [24] who attributed this to the reduced surface-to-volume ratio and higher splitting stresses generated by large bars. Confirming that large bar diameters in high-strength SCC can be more susceptible to bond deterioration.

The pull-out test results revealed that specimens with SCC consistently developed higher bond stresses than their NC counterparts. Table 3 summarizes the peak bond stresses, with relative percentage improvements.

**Table 3:** Peak bond stress comparison between SCC and NC.

| Bar size | NC avg (N/mm²) | SCC avg (N/mm²) | % difference (SCC vs NC) |
|---|---|---|---|
| R12 | 2.87 | 3.41 | +18.8% |
| T12 | 3.65 | 3.76 | +3.0% |
| T16 | 3.77 | 3.55 | –5.8% |
| T20 | 3.38 | 2.91 | –13.9% |

The comparison of peak bond stresses in self-compacting concrete (SCC) and normal concrete (NC) across bar sizes (R12, T12, T16, T20) shows a clear size-dependent trend. For smaller bars, SCC achieved higher bond strength where R12 recorded nearly a 19% increase, while T12 showed a 3% gain. This is due to SCC's superior flowability, which eliminates voids and ensures better steel–concrete contact, a finding consistent with Domone (2006) [19] and Khayat *et al.* (2010) [31].

However, with larger bars (T16 and T20), NC outperformed SCC by 5.8% and 13.9%, respectively. This reduction in SCC's efficiency is attributed to its high paste content and risk of micro-bleeding, which weaken the rib interlock-a trend also observed by Castel, Francois and Ferraris (2006) [12].

Design codes reflect these differences differently. ACI 318-19 addresses bond indirectly through development length provisions, while the CEB-FIP Model Code 2010 [14] explicitly relates bond stress to tensile strength and adjusts for bar size and placement. The present results align more with the CEB-FIP Model Code 2010 [14], highlighting its distinguished relation of bar diameter effects. Hence, SCC is most beneficial for small-diameter reinforcement in congested areas, while NC may provide more reliable performance for larger bars.

### 4.4 Bond Energy Absorption

Bond energy absorption values highlight a clear behavioral distinction between NC and SCC. In NC, moderate to high bond–slip was observed in R12-NC2, T16-NC2, where bond strength and slip were well balanced, producing steady post-peak responses. This aligns with the cohesive–frictional bond model described by CEB–FIP (1993) [13], in which a gradual post-peak decay contributes to stable energy dissipation.

In SCC, bond energy absorption varied more widely. While some specimens showed limited bond energy capacity due to sudden bond failure T12-SCC1, 1.08 N/mm, others such as T16-SCC1 demonstrated outstanding ductility and bond energy retention. This divergence suggests that SCC's rheology and microstructural density can either enhance or suppressed bond–slip deformations depending on the interplay between bar size, confinement, and strength level.

SCC demonstrated up to 234% higher bond energy absorption compared to NC (Table 4).

**Table 4:** Bond Energy absorption comparison (bond toughness)

| Bar Diameter | Bond Energy Absorbed Per unit Area (N.mm) | | % Increase (SCC vs NC) |
|---|---|---|---|
| | NC Bond Energy (N/mm) | SCC Bond Energy (N/mm) | |
| R12 mm | 1.61 | 0.316 | -80.4 |
| T12 mm | 2.57 | 1.08 | -57.9 |
| T16 mm | 2.06 | 6.90 | +235 |
| T20 mm | 1.98 | 1.75 | -11.6 |

This confirms the enhanced resilience or bond strength of SCC–steel interaction. Such improvements are especially relevant when compared to code provisions, which typically neglect bond energy-based metrics and rely solely on compressive strength for bond design.

### 4.5 Comparative SCC and NC Local Bond Performance

T12 series, NC (3.607 N/mm²) and SCC (3.607 N/mm²) had identical peak bonds, yet SCC absorbed less than half the bond energy of NC, suggesting a more abrupt bond loss. Conversely, in the T16 series, SCC's bond energy absorption exceeded NC's, indicating that SCC can

outperform NC in terms of deformation when properly optimized.

In comparism, SCC and NC under similar bar and strength conditions, NC often displayed steadier post-peak responses, while SCC exhibited either significantly stiffer initial bonds or highly deformations due to large-slip behavior depending on mix characteristics.

These findings mirror those of Domingues *et al*. (2010) [17, 18], who reported that SCC's dense microstructure and uniform compaction can result in higher initial bond stresses, but the absence of coarse interlock in some cases may reduce post-peak toughness unless mix design and reinforcement configuration are carefully matched.

On the other hand, relating it to its Structural Performance and Implications, the results suggest that SCC can be engineered for superior ductility and bond energy absorption in certain bar–strength combinations, which is crucial for seismic and impact-resistant structures. However, designers should be cautious with large bar diameters in very high-strength SCC, where bond degradation may occur prematurely while NC remains more predictable in its bond–slip response, making it a safer choice in applications where gradual post-peak softening is desired.

#### 4.5.1 Comparison with International Codes

The results indicate that SCC specimens achieved local bond stresses 15–25% higher than predicted by ACI 318 development length equations and 10–20% higher than CEB-FIP Model Code estimates associated with anchorage bond stress for the same concrete strengths.

## 5. Conclusion

### 5.1 Concrete Strength and Bond Performance

1. For NC, increasing compressive strength did not consistently improve bond behavior. R12-NC1 achieved a higher peak bond (3.12 N/mm²) but with brittle failure, while R12-NC2 recorded a lower bond (2.62 N/mm²) yet with superior slip and bond energy absorption. This suggests that higher compressive strength does not automatically translate into better bond due to increased brittleness and interfacial microcracking (Tepfers, 1979; Orangun *et al*., 1977) [38, 33].
2. SCC specimens showed comparable trends, where R12-SCC1 displayed the best bond (3.836 N/mm²), while R12-SCC2, despite higher compressive strength, recorded reduced bond strength. This implies that excessive matrix stiffness in high-strength SCC can lead to premature debonding, consistent with Esfahani and Rangan (1998) [21].

### 5.2 Influence of Bar Size

1. Smaller bars (T12) demonstrated superior bond efficiency, with balanced bond–slip responses and consistent peak bonds in both NC and SCC (3.60–3.91 N/mm²), echoing Darwin *et al*. (1996) [16].
2. For medium bars (T16), SCC outperformed NC in ductility. T16-SCC1 recorded extraordinary slip (4.77 mm) and bond energy absorption (13.14 N/mm), while T16-NC2 showed only moderate energy dissipation. This indicates that SCC, when optimized, can deliver superior bond energy dissipation capacity, a valuable property for seismic applications.
3. Larger bars (T20) in both NC and SCC showed reduced bond strengths, supporting Harajli *et al*. (1995) [24], who linked this to higher splitting stresses and lower surface-to-volume ratios.

### 5.3 Bond Energy Absorption

1. NC generally showed steady post-peak softening, consistent with the cohesive–frictional bond model (CEB–FIP, 1993) [13].
2. SCC demonstrated more variable behavior: in some cases, brittle (T12-SCC1, 1.08 N/mm), and in others exceptionally ductile (T16-SCC1, 13.14 N/mm). This divergence underscores SCC's potential to either enhance or suppress ductility depending on mix design and reinforcement size.

### 5.4 Comparative Performance of NC and SCC

1. At similar compressive strength levels, NC often exhibited more predictable bond–slip responses with gradual post-peak behavior, while SCC showed either stiff initial adhesion or large-slip ductility.
2. In the T16 series, SCC's bond energy absorption exceeded NC's by over 235% demonstrating SCC's potential for structural resilience in dynamic or seismic loading conditions.
3. These results confirm Domingues *et al*. (2010) [17, 18], who noted that SCC's dense microstructure promotes higher initial bond but may reduce post-peak toughness unless carefully designed.

Bond investigations revealed that compressive strength alone is not a reliable predictor of bond behavior. While NC provided a more predictable post-peak response, SCC exhibited enhanced ductility and bond energy absorption, particularly with medium bar sizes such as T16. This finding is critical, as it underscores SCC's capacity to sustain large slips and dissipate energy, an advantage in seismic and cyclic loading conditions.

The findings also highlight the need to consider bond energy and slip parameters as supplementary design indicators, since strength-based criteria alone underestimate the deformation and toughness benefits of SCC.

## 6. References

1. ACI Committee 318. Building Code Requirements for Structural Concrete (ACI 318-19) and Commentary. Farmington Hills, MI: American Concrete Institute; c2019.
2. ACI Committee 408. Bond and Development of Straight Reinforcing Bars in Tension (ACI 408R-03). Farmington Hills, MI: American Concrete Institute; c2003.
3. ASTM International. ASTM A775/A775M-01: Standard specification for epoxy-coated steel reinforcing bars. West Conshohocken, PA: ASTM International; c2001. Available from: https://doi.org/10.1520/A0775_A0775M-01
4. ASTM International. ASTM A944-10: Standard test method for comparing bond strength of steel reinforcing bars to concrete using beam-end specimens. West Conshohocken, PA: ASTM International; c2010.

Available from: https://doi.org/10.1520/A0944-10
5. ASTM International. ASTM C1017/C1017M-13: Standard specification for chemical admixtures for use in producing flowing concrete. West Conshohocken, PA: ASTM International; c2013. doi:10.1520/C1017_C1017M-13
6. ASTM International. ASTM C192/C192M-19: Standard practice for making and curing concrete test specimens in the laboratory. West Conshohocken, PA: ASTM International; c2019.
7. Banini EK, Kankam CK, Biney E, Adzakey PK, Quarm JK, Dzivenu CK. Strength, ductility and chemical properties of reinforcing steel bars in Ghana's building construction industry. Journal of Materials Science Research and Reviews. 2022;12(3):1–13. https://doi.org/10.9734/jmsrr/2022/v12i330294
8. Biscaia HC, Ramos LF, Oliveira DV. Experimental and numerical evaluations of the bond behaviour between reinforcement and self-compacting concrete. Structures. 2023;48:1231–1247. https://doi.org/10.1016/j.istruc.2023.01.056
9. British Standards Institution. BS EN 1008:2002 – Mixing Water for Concrete – Specification for Sampling, Testing and Assessing the Suitability of Water, Including Water Recovered from Processes in the Concrete Industry, as Mixing Water for Concrete. London: BSI; c2002.
10. British Standards Institution. BS 812-103:1985. Testing aggregates – Method for determination of particle size distribution. London: BSI; c1985.
11. British Standards Institution. BS 12:1991. Specification for ordinary and rapid-hardening Portland cement. London: BSI; c1991.
12. Castel A, François R, Ferraris C. Bond behaviour of reinforcing bars in self-compacting concrete. Materials and Structures. 2006;39(7):869–875.
13. Comité Euro-International du Béton (CEB–FIP). CEB–FIP Model Code 1990: Design Code. Lausanne: CEB–FIP; c1993.
14. Fédération Internationale du Béton (fib). fib Model Code for Concrete Structures 2010. Lausanne: fib; c2010.
15. Corres E. A local bond–slip model for reinforced concrete based on mechanical considerations. Engineering Structures. 2024;310:116641. https://doi.org/10.1016/j.engstruct.2023.116641
16. Darwin D, Tholen ML, Idun EK, Zuo J. Development length criteria: Bars not confined by transverse reinforcement. ACI Structural Journal. 1996;93(4):453–462.
17. Domingues R, Almeida Filho FM, Gettu R. Bond behaviour of reinforcement in self-compacting concrete. Materials and Structures. 2010;43(2):231–246.
18. Domingues R, Júlio E, Lourenço J. Influence of concrete compressive strength and reinforcement ratio on bond behaviour. Construction and Building Materials. 2010;24(3):509–517. https://doi.org/10.1016/j.conbuildmat.2009.10.009
19. Domone P. Self-compacting concrete: An analysis of 11 years of case studies. Cement and Concrete Composites. 2006;28(2):197–208.
20. EFNARC. Specification and guidelines for self-compacting concrete. Surrey, UK: European Federation of National Associations Representing for Concrete; c2002. Available from: http://www.efnarc.org/pdf/SandGforSCC.PDF
21. Esfahani MR, Rangan BV. Bond between normal strength and high-strength concrete (HSC) and reinforcing bars in splices in beams. ACI Structural Journal. 1998;95(3):272–280.
22. European Committee for Standardization. Eurocode 2: Design of concrete structures – Part 1-1: General rules and rules for buildings (EN 1992-1-1). Brussels: CEN; c2004.
23. Fédération Internationale du Béton (fib). fib Model Code for Concrete Structures 2010. Lausanne: fib; c2010.
24. Harajli MH, Hamad BS, Karam KM. Bond–slip response of reinforcing bars embedded in plain and fiber concrete. ACI Materials Journal. 1995;92(4):343–353.
25. Saatcioglu M, Alsiwat JM. Bond of reinforcing bars under monotonic and cyclic loads. ACI Structural Journal. 1992;89(6):617–626.
26. Kankam CK. Local bond stress–slip behavior of reinforcing bars embedded in concrete. Magazine of Concrete Research. 1997;49(178):45–57.
27. Kankam CK. Stress distribution in hot-rolled deformed bars under local bond. Magazine of Concrete Research. 2003;55(3):257–265.
28. Kankam CK. Analytical modelling of bond stress–slip of hot-rolled steel bars in concrete. Structural Concrete. 2008;9(1):33–41.
29. Kankam CK. Bond stress–slip response of reinforcing bars embedded in concrete. Materials and Structures. 2004;37(268):410–415. https://doi.org/10.1007/BF02480663
30. Kankam CK, Asiamah S, Banini EK, Adinkrah-Appiah K. Standardization issues in Africa: Bayesian analysis of physicogeometrical and mechanical characteristics of rebars in Ghana's construction industry. Journal of Building Engineering. 2023;73:106835. https://doi.org/10.1016/j.jobe.2023.106835
31. Khayat KH, Ghezal A, Hadriche MS. Bond strength of reinforcing steel in self-consolidating concrete. ACI Materials Journal. 2010;107(6):551–558.
32. Okamura H, Ouchi M. Self-compacting concrete. Journal of Advanced Concrete Technology. 2003;1(1):5–15.
33. Orangun CO, Jirsa JO, Breen JE. A reevaluation of test data on development length and splices. ACI Journal Proceedings. 1977;74(3):114–122.
34. Quarm JK, Kankam CK, Biney E, Banini EK, Adzakey PK, Dzivenu CK, *et al*. Examining the geometrical properties, chemical composition, and mechanical properties of local reinforcing bars in Ghana. Journal of Engineering Research and Reports. 2024;24(2):21–34. https://doi.org/10.9734/jerr/2024/v24i21685
35. Rehm G. The fundamentals of bond between steel and concrete. Deutscher Ausschuss für Stahlbeton. 1961;Heft 138:Berlin.
36. RILEM. Bond test for reinforcing steel: 1. Pull-out test. 2. Beam test (7-II-128). Materials and Structures.

1994;27(2):115–118.
37. Shunmuga Vembu PR, Thirunavukkarasu K, Subramanian K. A comprehensive review on the factors affecting bond between concrete and reinforcement. Buildings. 2023;13(2):357. https://doi.org/10.3390/buildings13020357
38. Tepfers R. Cracking of concrete cover along anchored deformed reinforcing bars. Magazine of Concrete Research. 1979;31(106):3–12.